REPRESENTATION OF PLASMA TEMPERATURES IN IRI

Vladimir Truhlik

Department of the Upper Atmosphere
Institute of Atmospheric Physics, Academy of Sciences of the Czech Republic
Praha, Czech Republic
Email : vtr@ufa.cas.cz

Outline

- Introduction
- Data
  - Measurement
    - Electron temperature (Te)
    - Ion temperature (Ti)
- Plasma temperatures
  - Simplified theoretical description
  - representation in IRI
    - Electron temperature
    - Ion temperature
- Summary

Introduction

- Understanding the properties of the ionized part in the Earth‘s outer atmosphere is important for studying many phenomena, especially the propagation of electromagnetic signals (man made – radio waves, GNSS or natural -VLF -whistlers, various emissions etc.)
- Most important parameters which we study (and model in IRI):
  - Electron density (Ne) including its integral (TEC) (parameter of main focus, influences propagation of radio waves – refraction, reflection)
  - Ion composition (e.g., waves - whistler mode – LHR Lower Hybrid Resonance – important mean ion mass)
  - Plasma temperatures (thermal balance, important for transfer of energy, plasma scale height etc.)
    - Electron temperature (Te)
    - Ion temperature (Ti)
  - Drifts , F1 and spread-F probability, Es probability etc.

Electron temperature measurement

- Incoherent Scatter Radar (presentation of dr. Zhang)
- Langmuir probe (in-situ measurements)

  (Mott-Smith and Langmuir, 1926)

  a) Planar
  b) Cylindrical
  c) Spherical

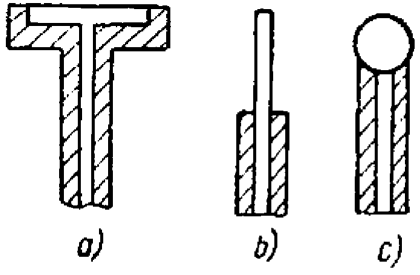

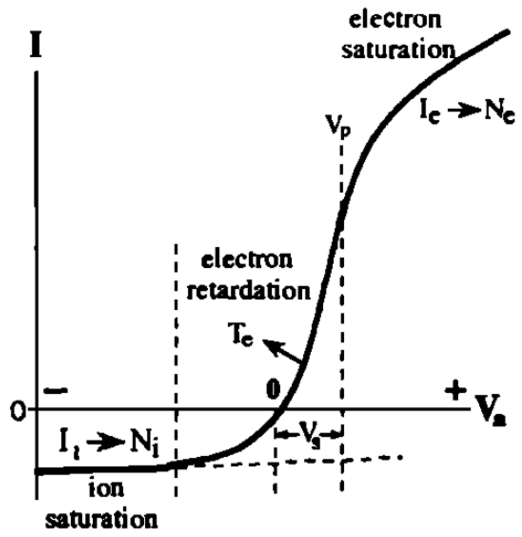

$$T_e \sim 11620 * (\Delta U / \Delta \ln(I))$$

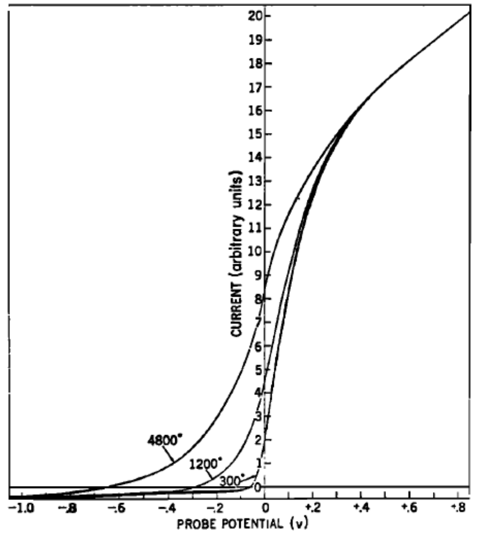

Maxwellian plasma

Both techniques often give different values!

Real LP experiments often measure higher values (even 2x) – contamination effect (difficult to keep the probe clean)

ISR does not suffer this problem (in non-thermal eq. plasma lower Te)

Ion temperature measurement

- Incoherent Scatter Radar (presentation of dr. Zhang)
- Retarding potential analyser or planar sensor (RPA, IVM) (in-situ measurements)
- Maxwellian plasma
- i-th ion flux

$$\phi_i(P) = \frac{N_i}{2} V_r \left[1 + erf(\beta_i f_i) + \frac{1}{\sqrt{\pi}\beta_i V_r} \exp(-\beta_i^2 f_i^2) \right]$$

$$\beta_i = \left({m_i}/{2kT_i} \right)^{1/2}$$

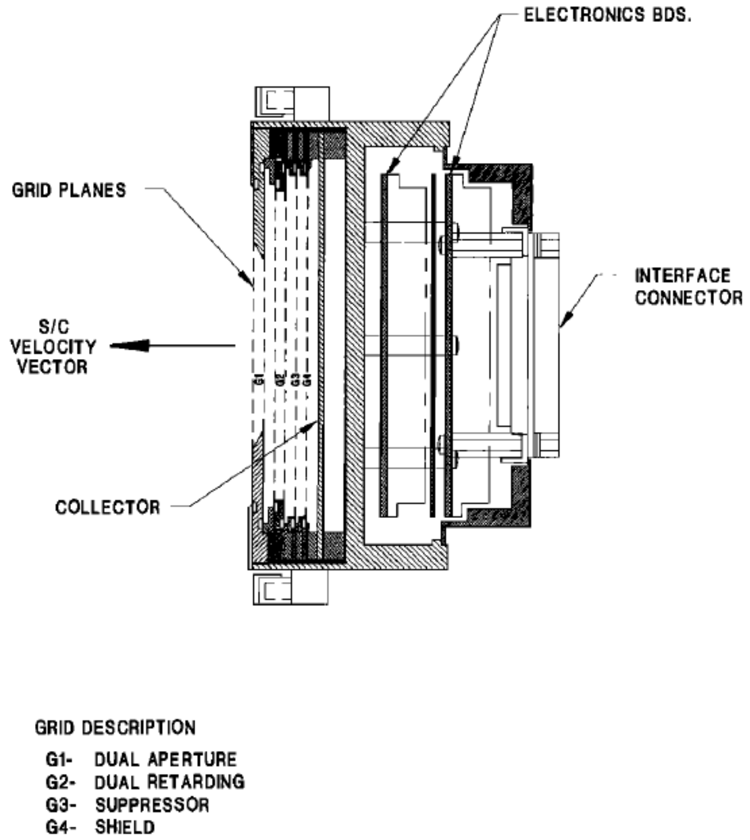

Temperature of all ions considered as the same

Complicated numerical procedure to obtain Ti – nonlinear fitting

Electron temperature

Equation of thermal balance (day, night – steady state – neglect changes with time)

$$\sin^2 I \frac{\partial}{\partial h}\left(K_e \frac{\partial T_e}{\partial h} \right) + \sum Q_e - \sum L_e = 0$$

Q_e – heating (from photoelectrons)

local <350km

non-local plasmaspheric

L_e – cooling – very complex – energy loss:

<350km neutral particles O, N_2(r,v), O_2 (r,v)

topside with ions O^+, H^+, He^+ (Coulomb)

K_e – thermal conductivity

I – inclination of the geomagnetic field

FLIP model - electron cooling rates in the equtorial region up to 350km as a function of altitude for various cooling terms (Coulomb —, rN2 —, rO2 —, vN2 —, vO2 —, fsO ……, O1D …..).

Coulomb cooling in the topside ionosphere is dominant

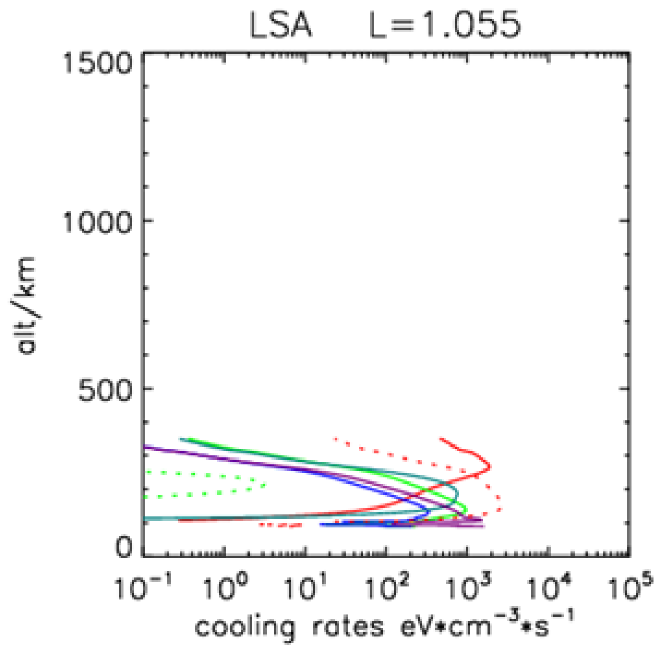

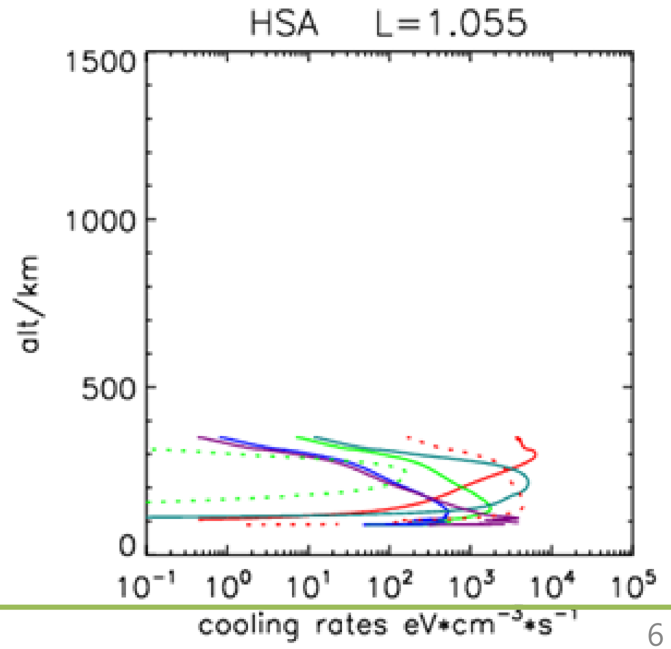

Te – altitude profiles in topside and plasmasphere

Thermal conductivity

$$K_e = 7.7 \times 10^5 T_e^{5/2}$$

Te profile – constant heat flux

$$T_e(h) = T_0[1 + 3.5\frac{G_0}{T_0}(h - h_0)]^{2/7}$$

Te_0, G_0 – electron temperature and gradient (e.g. at 500km)

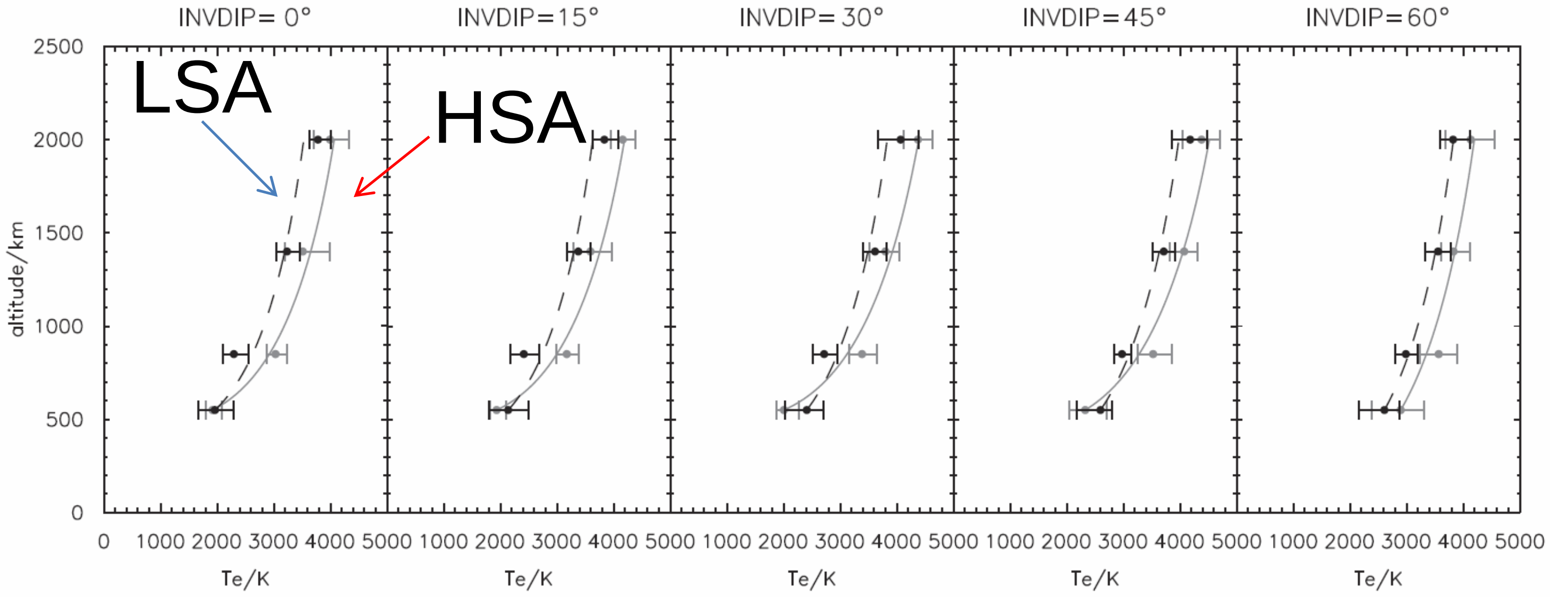

Ion temperature

Equation (neglect time changes, neglect heat flux)

$$\sum Q_i - \sum L_i = 0$$

Q_i – heating from electrons (Coulomb heating)

L_i – cooling:

neutral particles O, N_2, O_2

and other ions (O^+, H^+, He^+)

$aTi^3+bTi^2+cTi+d=0$

a,b,c,d depends on Te and Tn

Resonant charge exchange

Polarization reactions

Energy Loss Rates Due to Collisions of Ions with Neutrals

Ion Mixture	Energy Loss Rate, 10^{-14} eV cm^{-3} s^{-1}
O^+-N_2	$6.6n(O^+)n(N_2)(T_i - T_n)$
O^+-O_2	$5.8n(O^+)n(O_2)(T_i - T_n)$
O^+-He	$2.8n(O^+)n(He)(T_i - T_n)$
O^+-O	$0.21n(O^+)n(O)(T_i + T_n)^{1/2}(T_i - T_n)$
O^+-H	$0.36n(O^+)n(H)T_n^{1/2}(T_i - T_n)$
He^+-N_2	$5.3n(He^+)n(N_2)(T_i - T_n)$
He^+-O_2	$4.5n(He^+)n(O_2)(T_i - T_n)$
He^+-O	$5.8n(He^+)n(O)(T_i - T_n)$
He^+-H	$10.0n(He^+)n(H)(T_i - T_n)$
He^+-He	$0.4n(He^+)n(He)(T_i + T_n)^{1/2}(T_i - T_n)$
H^+-N_2	$3.1n(H^+)n(N_2)(T_i - T_n)$
H^+-O_2	$2.8n(H^+)n(O_2)(T_i - T_n)$
H^+-He	$5.5n(H^+)n(He)(T_i - T_n)$
H^+-H	$1.4n(H^+)n(H)(T_i + T_n)^{1/2}(T_i - T_n)$
H^+-O	$0.40n(H^+)n(O)T_n^{1/2}(T_i - T_n)$
NO^+-O_2	$5.45n(NO^+)n(O_2)(T_i - T_n)$
NO^+-N_2	$5.916n(NO^+)n(N_2)(T_i - T_n)$
NO^+-O	$4.5n(NO^+)n(O)(T_i - T_n)$
O_2^+-N_2	$5.807n(O_2^+)n(N_2)(T_i - T_n)$
O_2^+-O	$4.358n(O_2^+)n(O)(T_i - T_n)$
O_2^+-O_2	$0.14n(O_2^+)n(O_2)(T_i + T_n)^{1/2}(T_i - T_n)$

The data here are from *Banks* [1966*b*].

Rees and Roble, Rev. Geoph. and Sp. Ph., 1975

IRI Te model

- Bil-1985- based on Brace and Theis Te maps (JASTP 1981)
  – coordinates diplat and solar local time
- TTSA option (JASR 2001) replaced by new TBT-2012 (EPS, 2012)
- IRI2012/IRI2016
  – JF(2)-.true./.false. - Te,Ti computed/not computed
  – JF(23)-.true./.false.-Bil-1985/TBT-2012
- Ne/Te correlation (Brace and Theis, 1978)
  - JF(10) -.true./.false.-Te – Standard /Te - Using Te/Ne correlation

Ne-Te correlation

$$T_e = P_1 + (P_2 h + P_3) \exp(P_4 h + P_5 N_i + P_6 h N_i) \quad (1$$

where
T_e is in units of °K
N_i is in units of cm^{-3}
h is in kilometers.

The best fit was obtained using the following coefficients,

$P_1 = 1.051 \times 10^3$
$P_2 = 1.707 \times 10^1$
$P_3 = -2.746 \times 10^3$
$P_4 = -5.122 \times 10^{-4}$
$P_5 = 6.094 \times 10^{-6}$
$P_6 = -3.353 \times 10^{-8}$

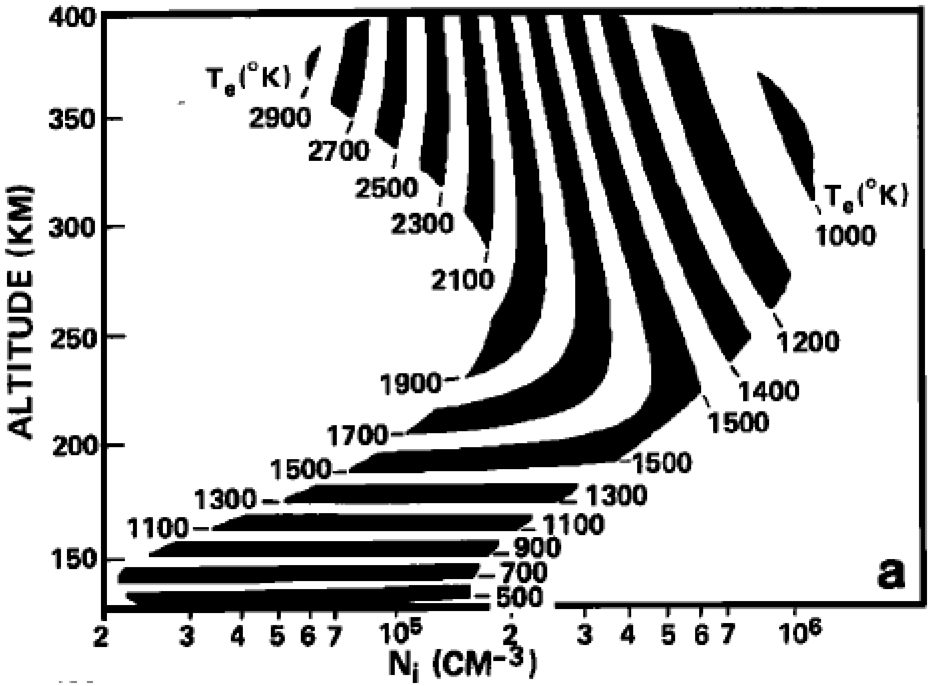

Brace and Theis, 1978

IRI 300 and 400km

Ne/Te correlation

validity?

Hinotori,
daytime,
equatorial
latitudes

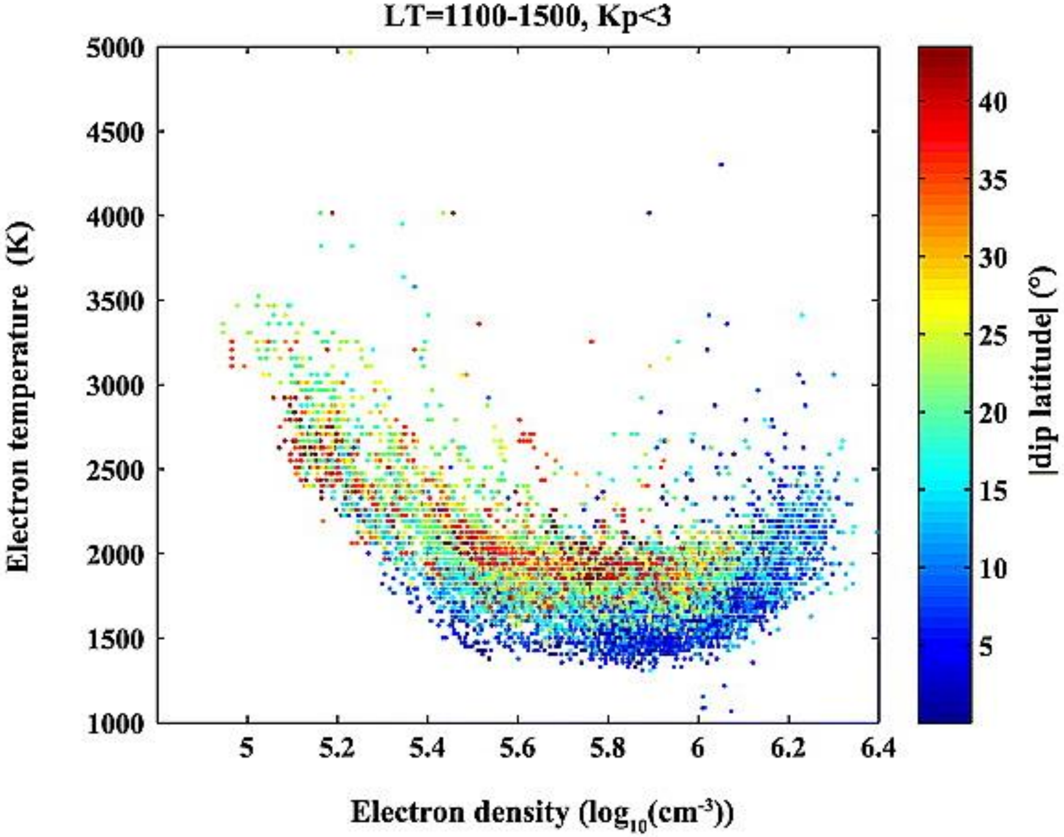

Kakinami et al., JGR 2011
“U” shape

TBT-2012 Te model

- Employs the all available satellite Te data
- Include solar activity variation for day and night - an example for 550km and equinox:

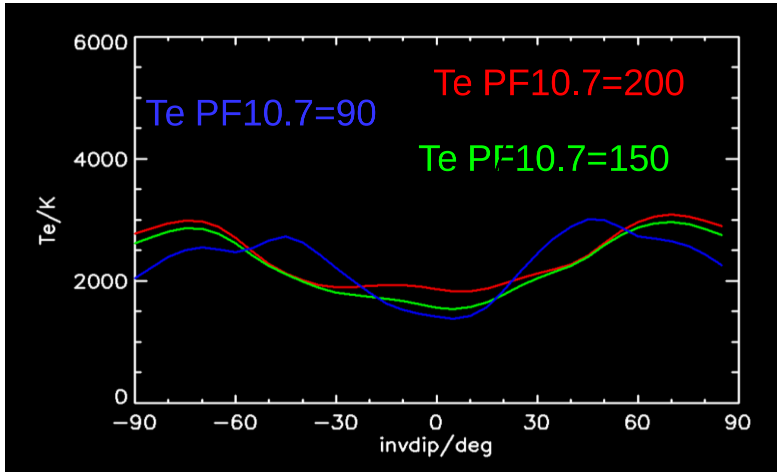

Corrected Te model

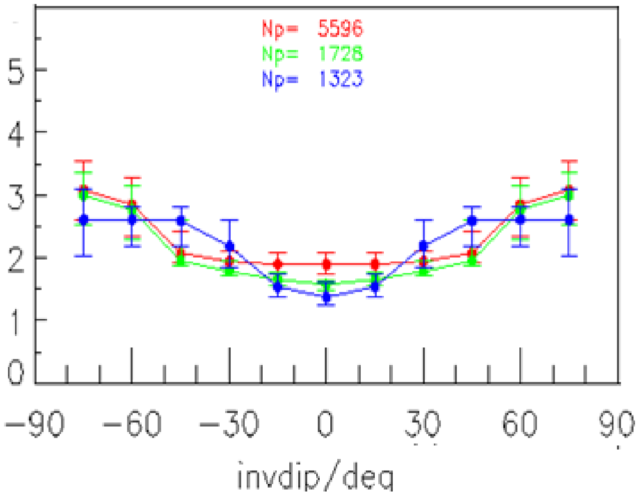

Data empirical profile

- Employs minimum of independent coordinates
  - to solve problem of limited data coverage
- Longitudinal structure neglected when it is used latitude coordinate based on the configuration of the real magnetic field
  - coordinates invdip and magnetic local time

Magnetic latitude coordinates

- diplat:

$$diplat = \arctan \frac{\tan(I)}{2}$$

where I is the dip angle or magnetic inclination

-longitudinal variation of Te reduced in equatorial latitudes

- Invariant latitude – invl (e.g. Roederer 1970):

$$L \cos^2 invl = R$$

where the invariant radius R and the McIlwain L parameter obey

$$B = \frac{M}{R^3}\left(4 - \frac{3R}{L}\right)^{\frac{1}{2}}$$

-longitudinal variation of Te reduced at mid-latitudes (Smilauer and Afonin, ASR 1985) – plasma distributed along magnetic field lines

- invdip – combination of diplat and invl (Truhlik et al. 2001):

$$invdip = \frac{\alpha\, invl + \beta\, diplat}{\alpha + \beta} \qquad \alpha = \sin^3 |diplat| \text{ and } \beta = \cos^3 (invl)$$

invdip (or invdiplat)

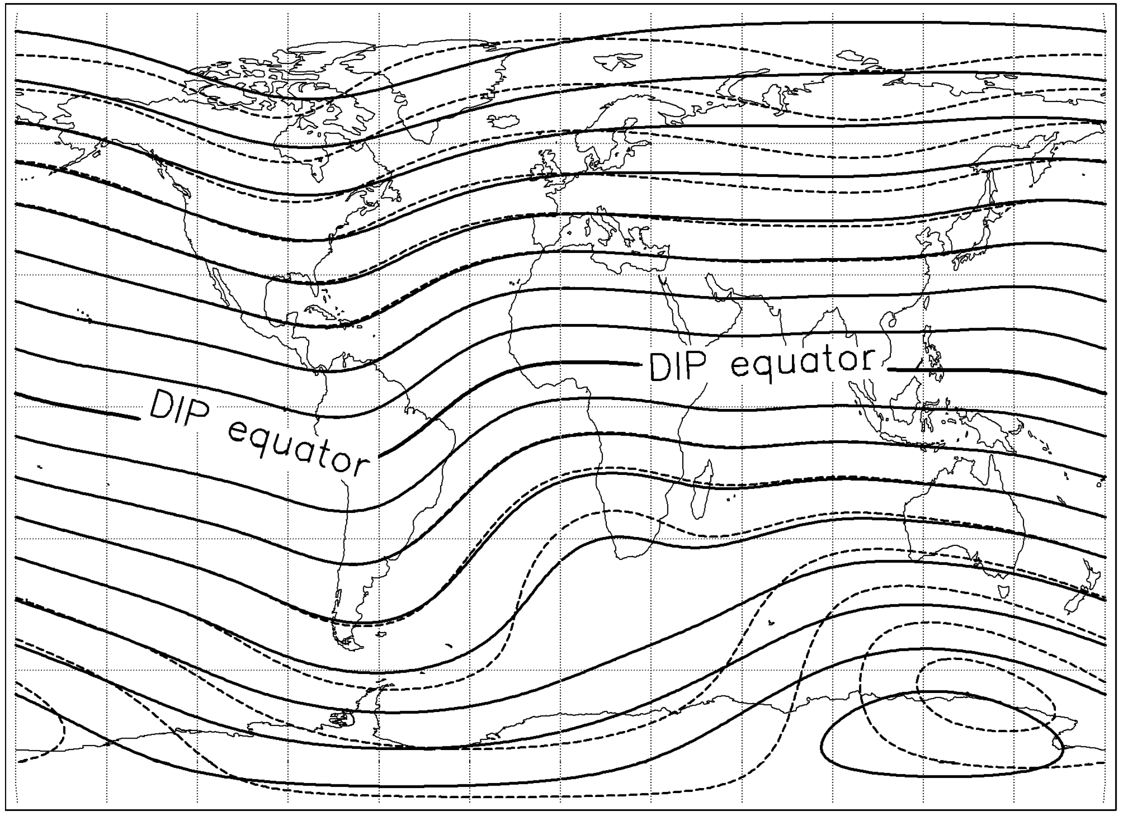

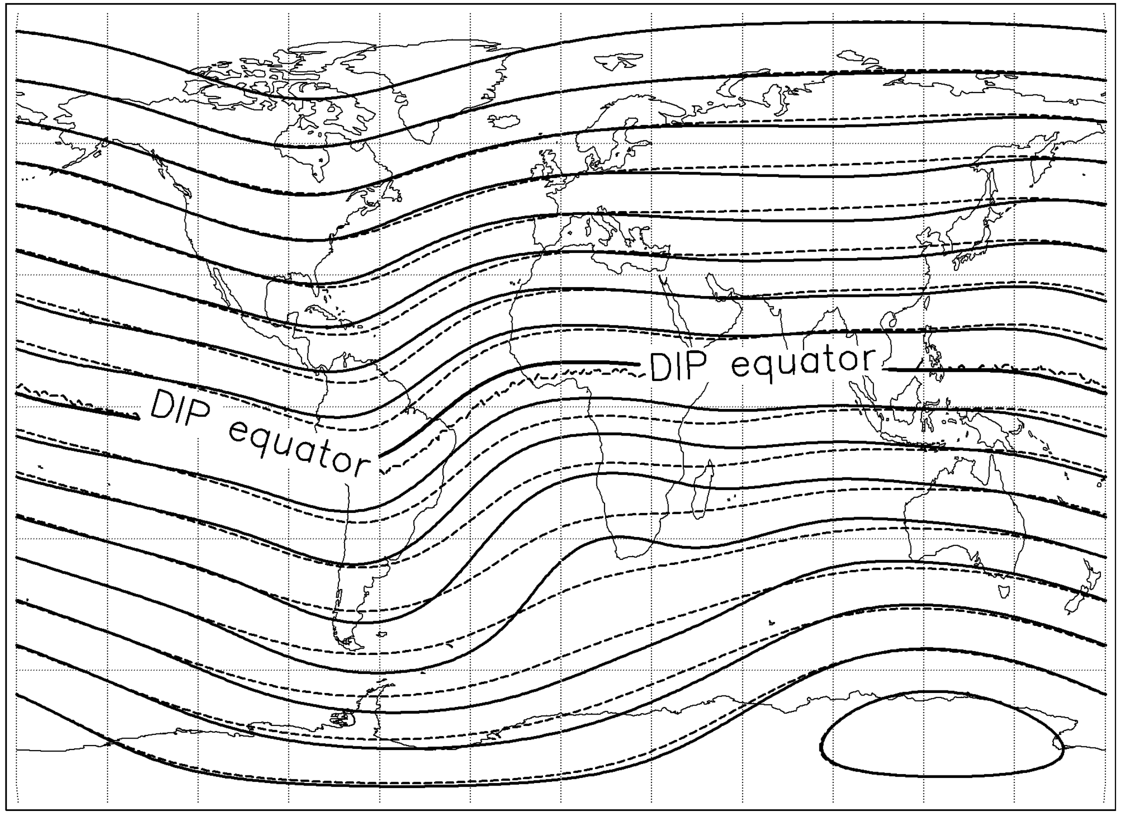

—— invdip – – – dip latitude

—— invdip – – – invariant latitude

Configuration of the real geomagnetic field (IGRF 1990 at 600km) in different latitude coordinates in steps of 10°

Te data (Data base – satellite data)

An example for the electron temperature - all available Te satellite data (source mainly SPDF, Madrigal)

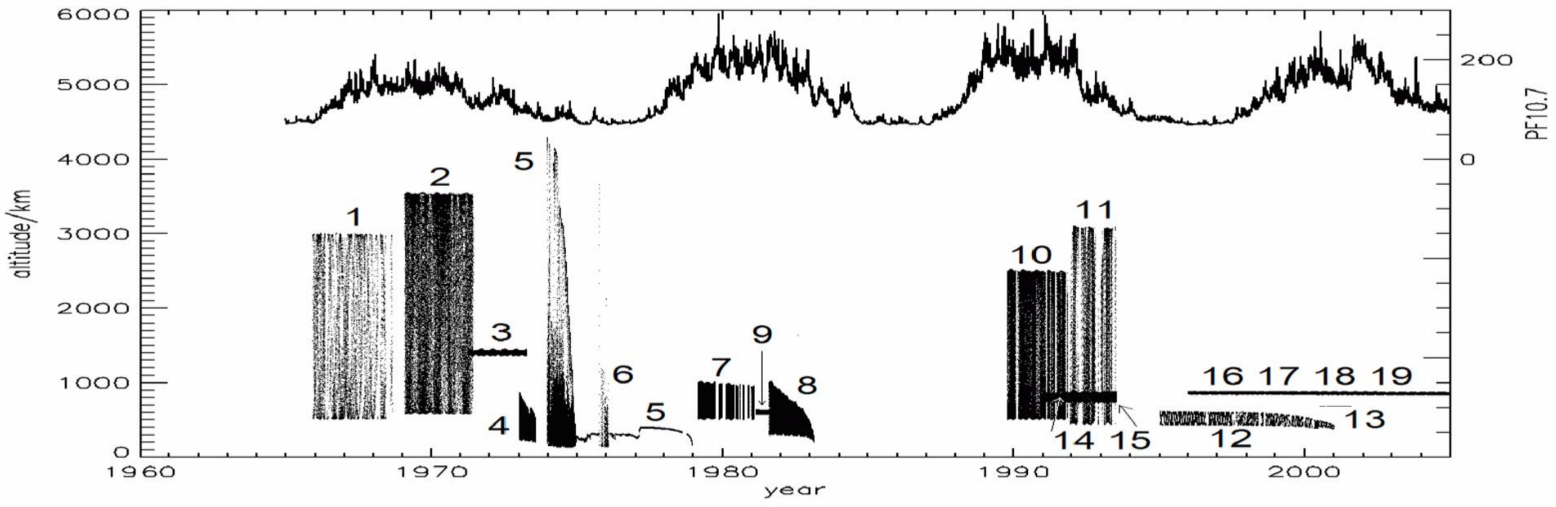

No.	Satellite	Time period	Altitude [km]	Latitude [deg]	LT [h]
1	Explorer 31 (DME-A)	11. 1965–8. 1968	500–3010	−79–79	0–24
2	ISIS-1	1. 1969–5. 1971	580–3550	−88–88	0–24
3	ISIS-2	4. 1971–3. 1973	1360–1460	−88–88	0–24
4	AEROS A	1. 1973–8. 1973	200–870	−83–83	3, 15 fixed
5	AE-C	12. 1973–12. 1978	130–4300	−68–68	0–24
6	AE-D	10. 1975–1. 1976	140–3700	−90–90	0–24
7	IK19	3. 1979 – 1. 1981	500 – 1020	−74–74	0–24
8	DE-2	8. 1981–2. 1983	200–1020	−90–90	0–24
9	Hinotori	2. 1981–6. 1982	560–640	−31–31	0–24
10	IK24	10. 1989–11. 1991	500–2530	−83–83	0–24
11	IK25	12. 1991–6. 1993	440–3110	−83–83	0–24
12	SROSS C2	1. 1995–12. 2000	380–620	−46–46	0–24
13	KOMPSAT	6. 2000 – 8. 2001	appx. 685	−90–90	22.8
14	DMSP F10	12. 1990–6. 1993	730–860	−90–90	8–20 fixed
15	DMSP F11	12. 1991–6. 1993	850–870	−90–90	5–17 fixed
16	DMSP F12	1. 1996–6. 2002	840–890	−90–90	9.5, 21.5
17	DMSP F13	3. 1995–12. 2005	840–880	−90–90	5.75,17.75
18	DMSP F14	1. 1997–12. 2005	840–880	−90–90	9.5, 21.5
19	DMSP F15	12. 1999–12. 2005	830–880	−90–90	9.5, 21.5

Year-altitude coverage of the data sets include in our data base. The curve at the top shows the solar 10.7 cm radio flux (F10.7 index – 3 months average).

Te model - Data distribution

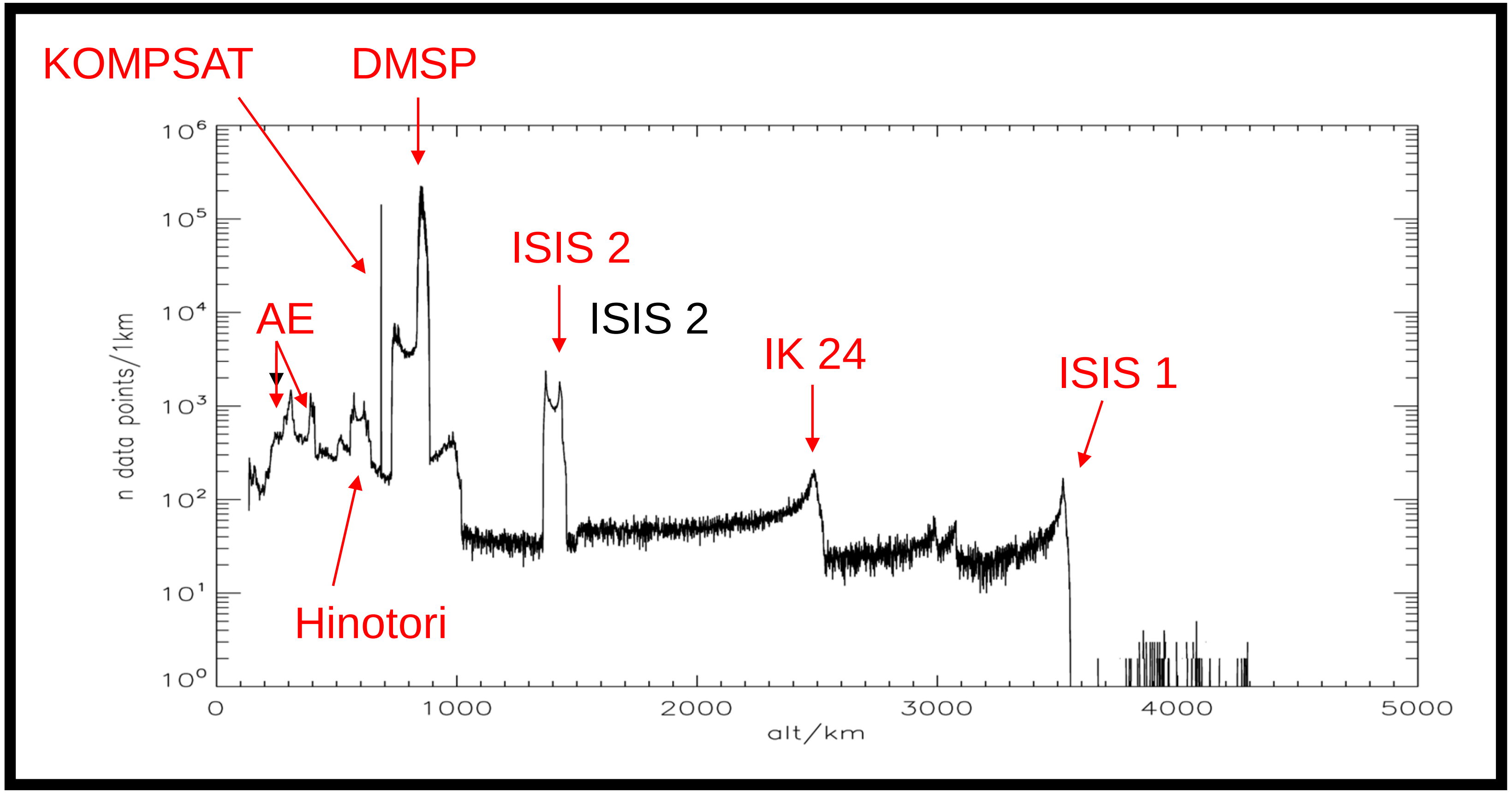

9 million points – non-uniform distribution
Peaks correspond to circularly orbiting satellites

Main (core) Te model

equinox

solstice

350km

550km

850km

1400km

2000km

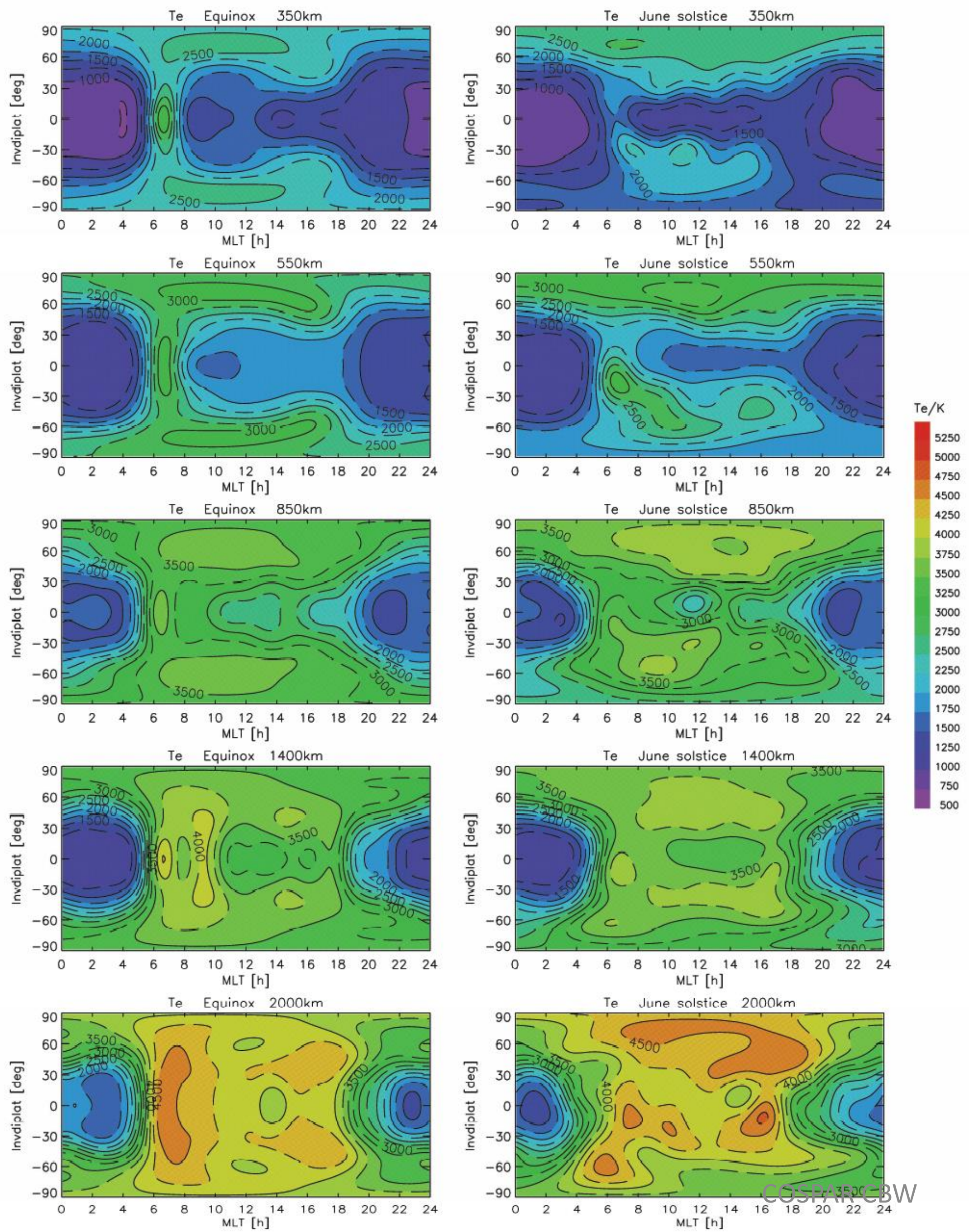

Data grouped - altitudes: 350, 550, 850, 1400 and 2000km

seasons: equinox, solstice

$$\log(Te_0) = a_0^0 + \sum_{l=1}^{8}\left\{ a_l^0 P_l^0(\cos\theta) + \sum_{m=1}^{l}\left[a_l^m \cos m\varphi + b_l^m \sin m\varphi \right] P_l^m(\cos\theta) \right\}$$

A system of associated Legendre polynomials up to the 8th order was employed.

P_l^m = associated Legendre function

θ = invdip colatitude ($0..\pi$)

ϕ = magnetic local time ($0..2\pi$).

-Te increases with altitude.

- At low latitudes (±30 invl) during the nighttime the Te altitude gradient is very small.

- Morning enhancement (morning overshoot) at equatorial latitudes and at low altitudes (350, 550 to 850 km)

- For solstices its maximum is shifted to the the winter hemisphere

- Dependence on invariant latitude is more prominent at lower altitudes (350 to 850 km).

- Generally the lowest electron temperature is observed close to the equator and increases with increasing invariant latitude.

Solar activity variation of Te

Both Q_e (heating rate) and L_e (cooling rate) depend on solar activity – increase with increasing solar activity

$$\Downarrow$$

Te can increase, decrease or stay constant with increasing solar activity depending on altitude, latitude, local time and season!

Description of solar activity influence

- Problem - Te variation with solar activity is very close to the Te scatter or the error of the Te measurement => we need a very robust solution not to introduce 'artificial' variation
- Model driven by PF10.7 index *=(F10.7_81days_average+F10.7_daily)/2*
- Normalized latitude profiles of Te for 3 levels of solar activity for day (13h MLT) and night (1h MLT):

  a) low PF10.7 < 110

  b) medium 110 <= PF10.7 < 180

  c) high F10.7=>180)
  - Quadratic fit inside 110 <= PF10.7 < 180; Outside linear extrapolation
  - Local time dependence approximated by a harmonic function
  - Obtain a correction function TePF107(mlt,invdip,PF107)
- Thus, for fixed altitude we have the whole model: Te(mlt,invdip,PF107)=Te(mlt,invdip)+TePF107(mlt,invdip,PF107)

Latitude profiles of Te

high medium low solar activity

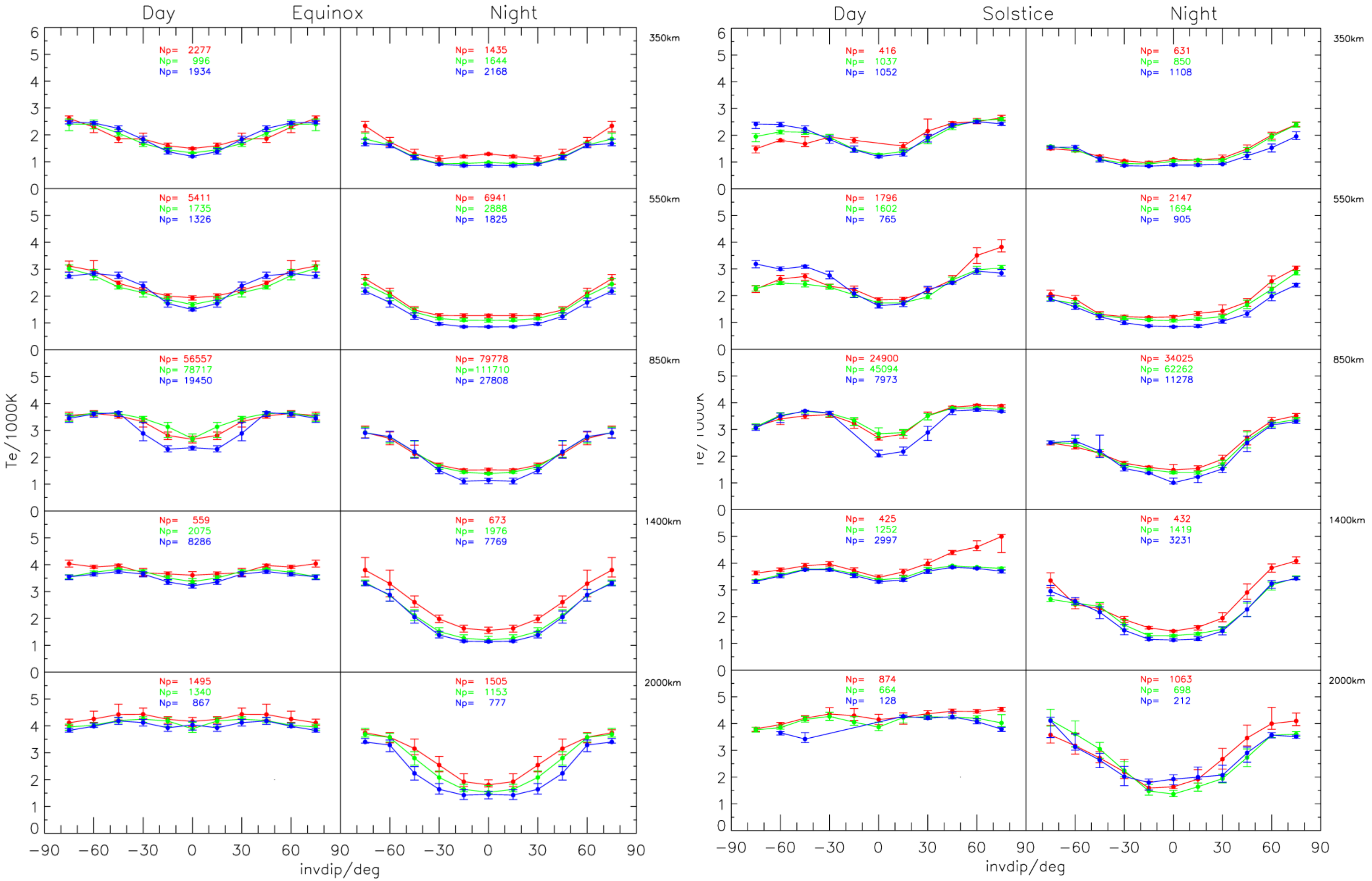

Ti IRI-2020

- Two options
  - The TBKST-2021 Ion Temperature Model
  - The Bil-1981 Ion Temperature Model
  - JF(2)-.true./.false. - Te,Ti computed/not computed
  - JF(48)-.true./.false.-TBKST-2021 (default) /Bil-1981

Description of Ti in IRI-2016 Bil-1981

- Altitude profiles constructed as follows (e.g. Bilitza, 1990, Pignalberi et al. 2020):
  - at an altitude of 200 km Ti = Tn
    - Tn from NRLMSIS00 (includes solar activity variation of Tn)
  - 430 km Ti from the AEROS A model (latitudinal profiles for day and night, Bilitza 1981)
  - Above 430 km a gradient from ISR (Arecibo and Millstone Hill) data
- Tn <= Ti <=Te – imposed

IRI-2016

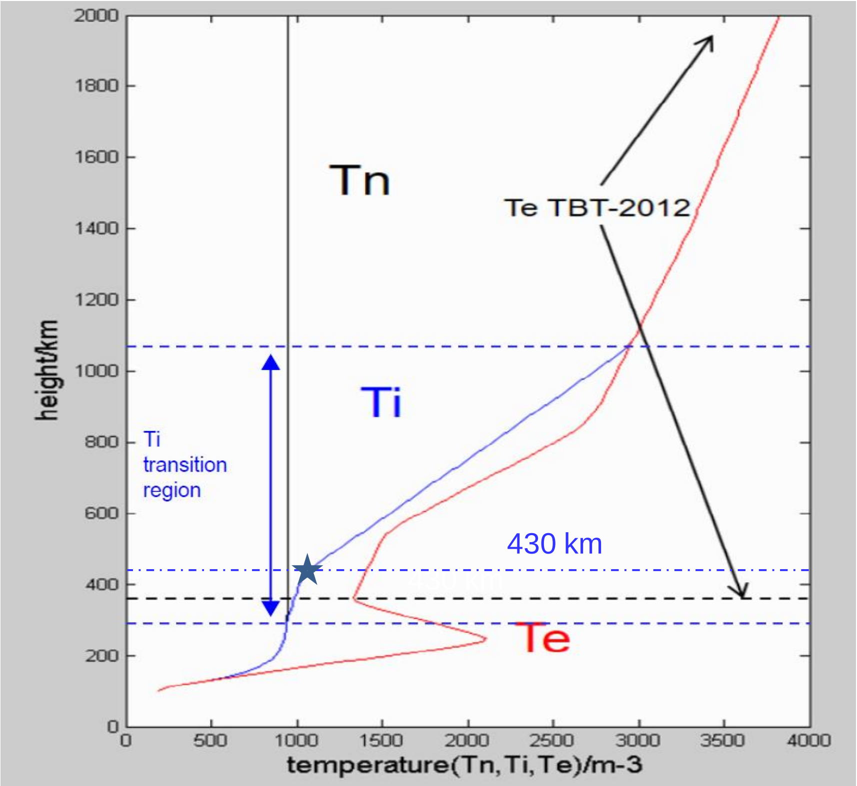

Altitude profiles of ion, electron and neutral temperatures (Ti, Te, and Tn) as modelled by IRI. The Ti transition region describes the part of the profile, where Ti deflects from Tn at low altitudes and merges with Te at higher altitudes.

New Ti model (option) in IRI-2020

-Calibrated data using ISR, fixed altitude (350, 430, 600, 850 km – transition region)
(above 1000 km poor data coverage)

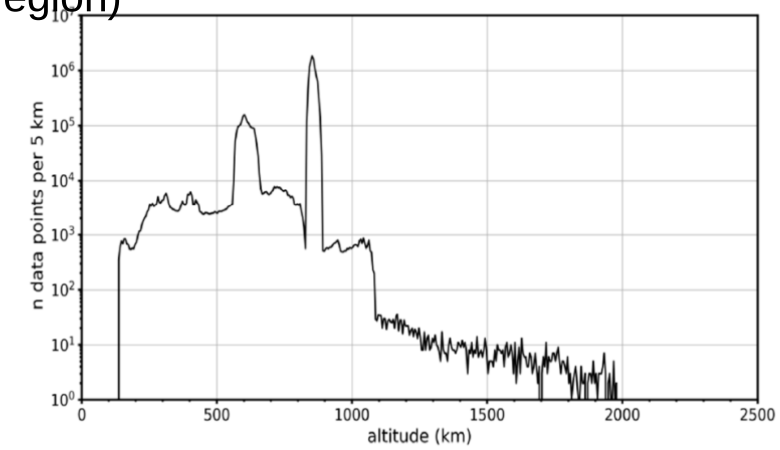

-Modelling coordinates
Latitude (invdip) and MLT
-Seasons
equinox, solstice
(no hemispheric differences)
-Modeling grid 9x18=162 bins

-Spherical harmonics (orthogonal system) up to 8th order

$$Ti_{main}(invdip, MLT) = \sum_{l=0}^{8}\left\{a_l^0 P_l^0\left(\cos\theta\right) + \sum_{m=1}^{l}\left[a_l^m \cos m\varphi + b_l^m \sin m\varphi\right]P_l^m\left(\cos\theta\right)\right\}$$

P_l^m = associated Legendre function
θ = invdip colatitude (0..π)
ϕ = magnetic local time (0..2π).

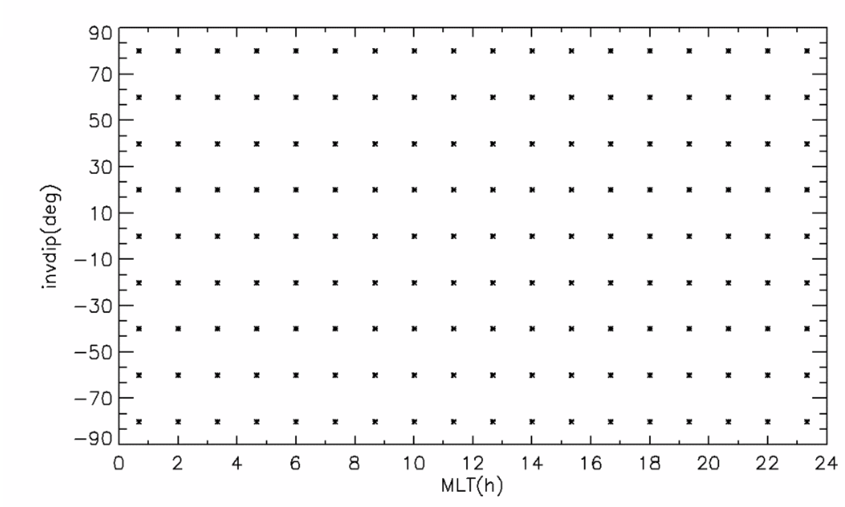

Data - ion temperature

- Available satellite data
  - (SPDF, Madrigal, etc.)
    - Data base of Ti
    - 100s data averages
      - 13,673,200 points

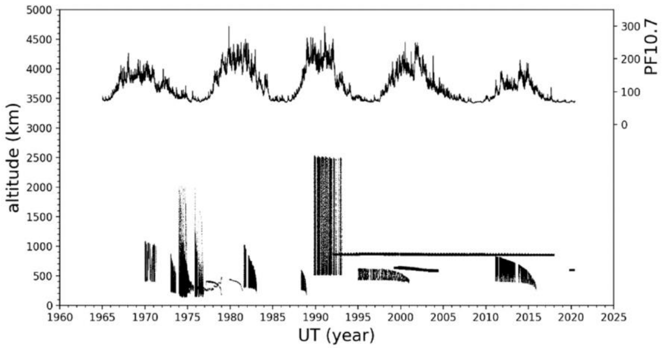

Year–altitude coverage of data in the database for individual satellite missions and corresponding 81-day running mean of the F10.7 index.

No	Satellite (Experiment)	Time Period (Data Avail)	Altitude [km]	Latitude [deg]	SLT [h]	$\overline{PF10.7}$
1	OGO-6 (RPA)	12. 1969–4. 1971	390–1090	−82 .. +82	0–24	155
2	AEROS A (RPA)	1. 1973–8. 1973	200–870	−83 .. +83	3, 15 fixed	98
3	AEROS B (RPA)	7. 1974–9. 1975	140–880	−83 .. +83	4, 16 fixed	86
4	AE-C (RPA)	12. 1973–12. 1978	135–2010	−68 .. +68	0–24	86
5	AE-D (RPA)	10. 1975–1. 1976	140–1980	−89 .. +89	0–24	76
6	AE-E (RPA)	12. 1975–5. 1981	140–1580	−20 .. +20	0–24	129
7	DE-2 (RPA)	8. 1981–2. 1983	200–1020	−90 .. +90	0–24	180
8	San Marco 5 (RPA)	4. 1988–12. 1988	170–590	−3 .. +3	0–24	151
9	IK24 (RPA)	10. 1989–2. 1993	500–2525	−83 .. +84	0–24	195
10	DMSP F11 (RPA)	1. 1992–5. 2000	840–890	−81 .. +87	6, 18 fixed	119
11	DMSP F12 (RPA)	1. 1996–6. 2002	840–890	−82 .. +89	9, 21 fixed	132
12	DMSP F13 (RPA)	3. 1995–12. 2005	840–880	−81 .. +82	6, 18 fixed	131
13	DMSP F14 (RPA)	4. 1997–7. 2003	840–885	−81 .. +82	9, 21 fixed	121
14	DMSP F15 (RPA)	12. 1999–12. 2017	830–880	−86 .. +86	9.5, 21.5 fixed	116
15	SROSS C2 (RPA)	1. 1995–12. 2000	380–620	−40 .. +45	0–24	110
16	ROCSAT-1(RPA)	3. 1999–6. 2004	560–665	−35 .. +35	0–24	160
17	C/NOFS (RPA)	8. 2008–11. 2015	260–855	−13 .. +13	0–24	106
18	ICON IVM (RPA)	10. 2019–6. 2020	575–610	−27 .. 27	0–24	70

Table: A list of the satellites and experiments included in the database and their corresponding time intervals, altitude, latitude, and solar local time (SLT) ranges, and the average PF10.7 index.

Data quality assessment

ISR	g)	Invdip (deg)
Jicamarca		0.0 ± 0.6
Arecibo		28.2 ± 2.2
Millstone Hill		52.8 ± 2.1

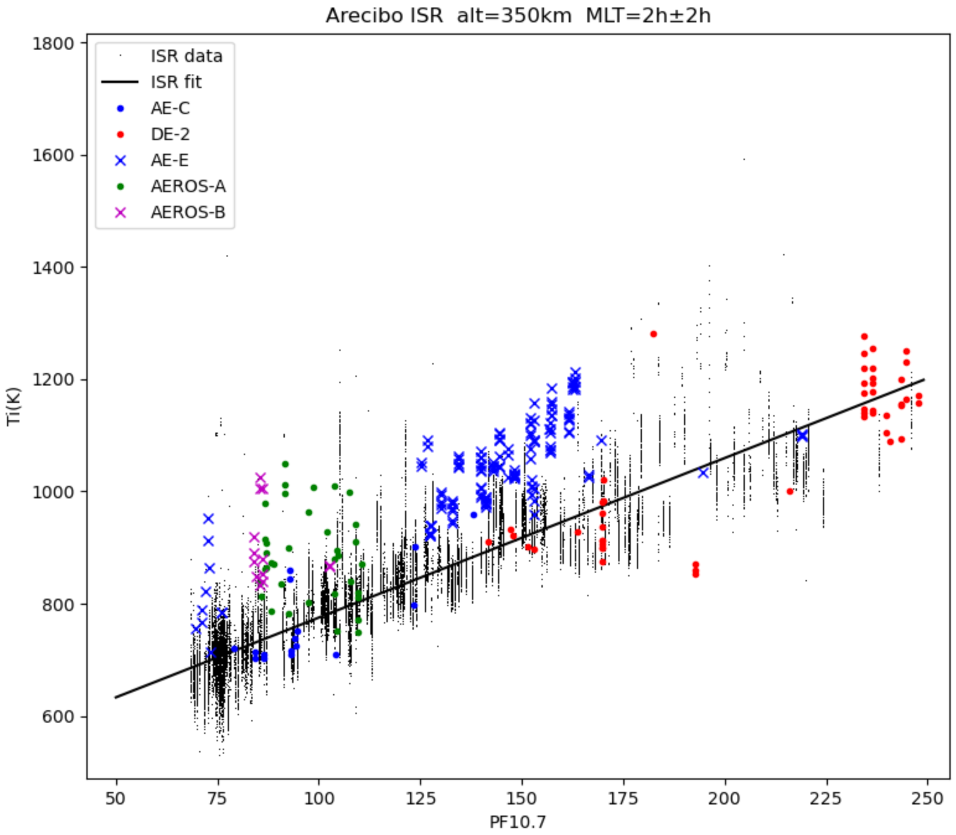

Example for 350km and night
DE-2 and AE-C follow the Arecibo linear fit
AE-E, AEROS-A, AEROS-B slightly above

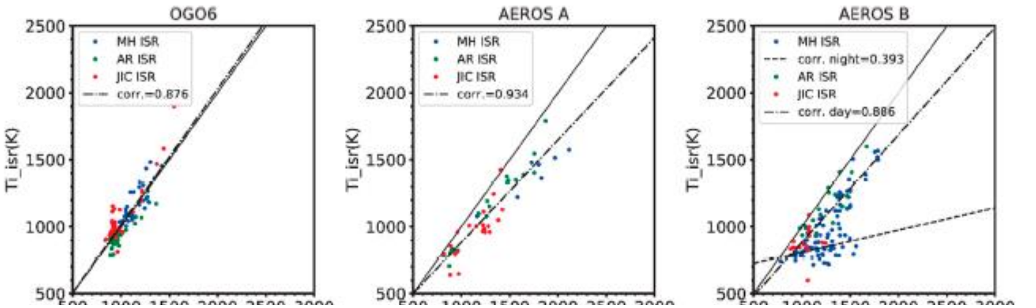

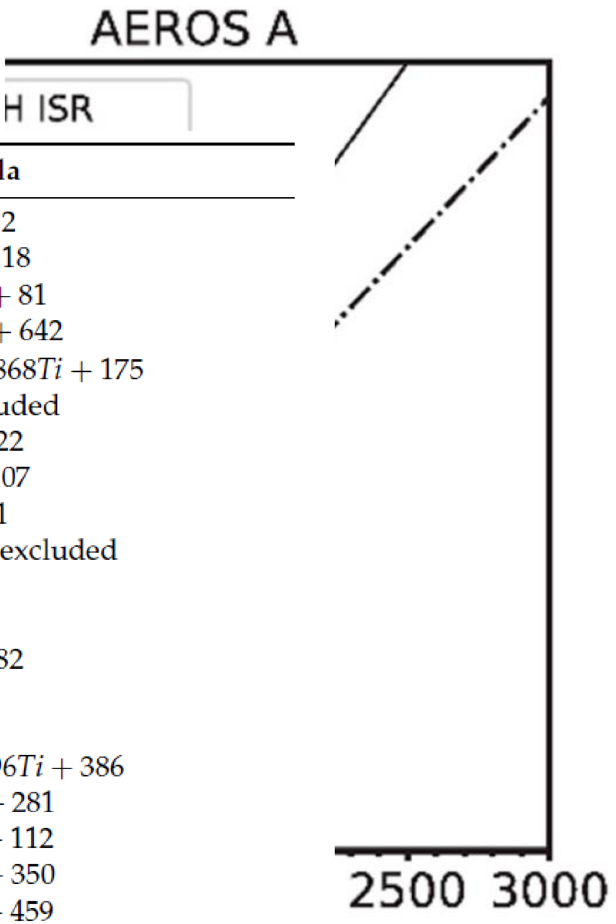

Binned all Ti data from each satellite
±5° invdip range centered at the pos
of each ISR (0°, 28.2°, and 52.8°) an
Binned all Ti dat
to the parameter
– Four seasons
June 21, Septen
and extending 3
– Six altitudes (
km, 450 km, 500
extending 10% a
given altitude);
– Twenty-four m
(centered at 0.5
and within ±0.5
– Twelve levels
centered at 72.5
±7.5 s.f.u.).

No	Satellite (Experiment)	Correction Formula
1	OGO-6 (RPA)	$Ti_{corr} = 1.015Ti - 2$
2	AEROS A (RPA)	$Ti_{corr} = 0.765Ti + 118$
3	AEROS B (RPA)	$Ti_{corr\_day} = 0.803Ti + 81$ $Ti_{corr\_night} = 0.166Ti + 642$
4	AE-C (RPA)	$Ti_{corr} = -0.0000865Ti^2 + 0.868Ti + 175$
5	AE-D (RPA)	No coincidences-excluded
6	AE-E (RPA)	$Ti_{corr} = 0.936Ti - 22$
7	DE-2 (RPA)	$Ti_{corr} = 0.848Ti + 107$
8	San Marco 5 (RPA)	$Ti_{corr} = 1.0Ti + 21$
9	IK24 (RPA)	Not enough coincidences-excluded
10	DMSP F11 (RPA)	
11	DMSP F12 (RPA)	
12	DMSP F13 (RPA)	$Ti_{corr} = 0.844Ti + 82$
13	DMSP F14 (RPA)	
14	DMSP F15 (RPA)	
15	SROSS C2 (RPA)	$Ti_{corr} = 0.000189Ti^2 + 0.396Ti + 386$
16	ROCSAT-1(RPA)	$Ti_{corr\_JIC} = 0.785Ti + 281$ $Ti_{corr\_AR} = 0.955Ti + 112$
17	C/NOFS (RPA)	$Ti_{corr\_JIC} = 0.641Ti + 350$ $Ti_{corr\_AR} = 0.543Ti + 459$
18	ICON IVM (RPA)	$Ti_{corr} = 0.648Ti + 173$

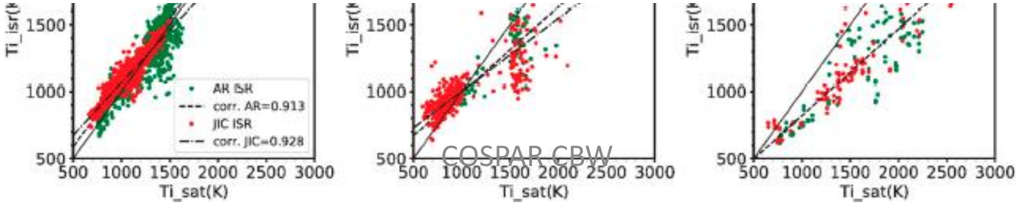

Solar activity term

$$Ti(invdip, MLT) = Ti_{main}(invdip, MLT) + Ti_{solact}(PF10.7, invdip, MLT)$$

$$Ti_{solact}(PF10.7, invdip, MLT) = a_{lin} PF10.7 + b_{lin} + \\ + a_{qua} PF10.7^2 + b_{qua} PF10.7 + c_{qua}$$

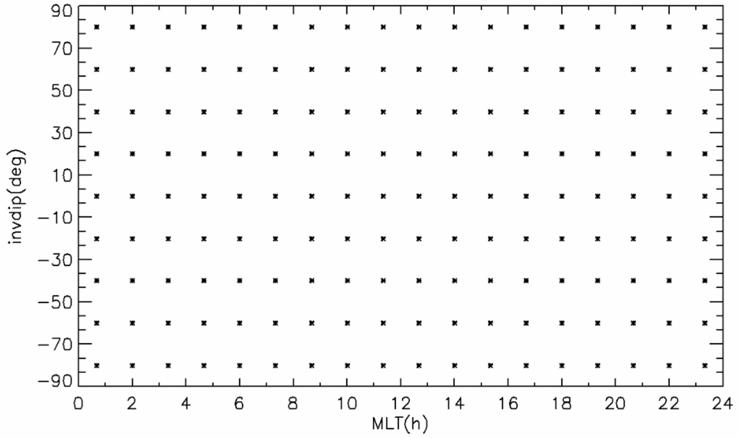

350 km, 430 km – linear term most important
600 km, 850 km – dawn, dusk, day and low latitudes second order
i.e., quadratic term important ("U shape" like dependence etc.)

a_{lin}, b_{lin}
a_{qua}, b_{qua}, c_{qua}
Spherical harmonics expansion on the same grid as coefficients of the main model

350km 600km 850km

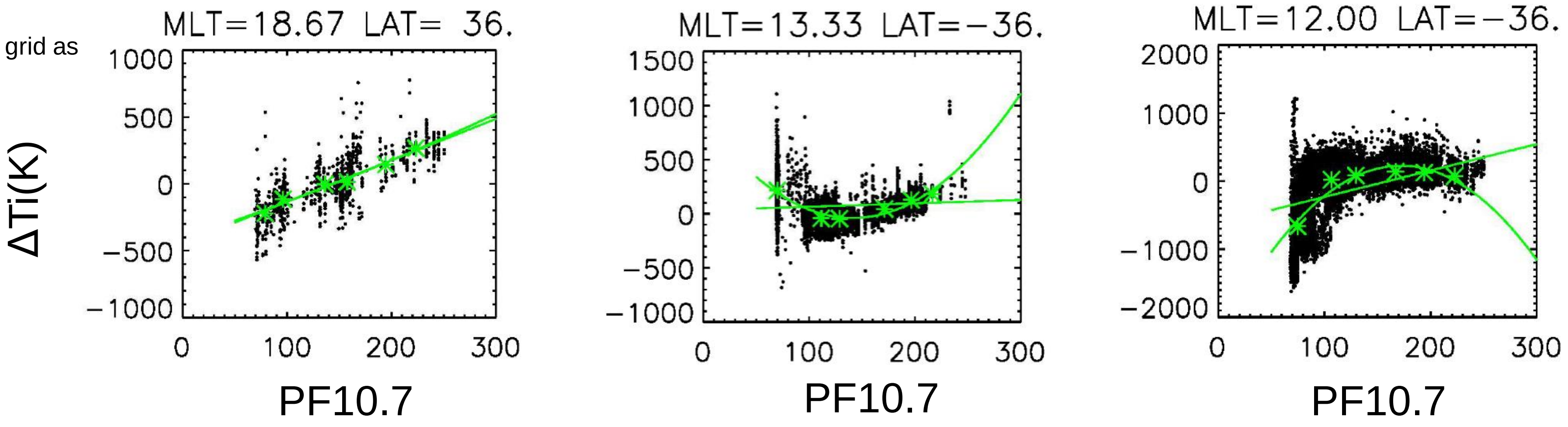

solar minimum (PF10.7=70) solar maximum (PF107=200)

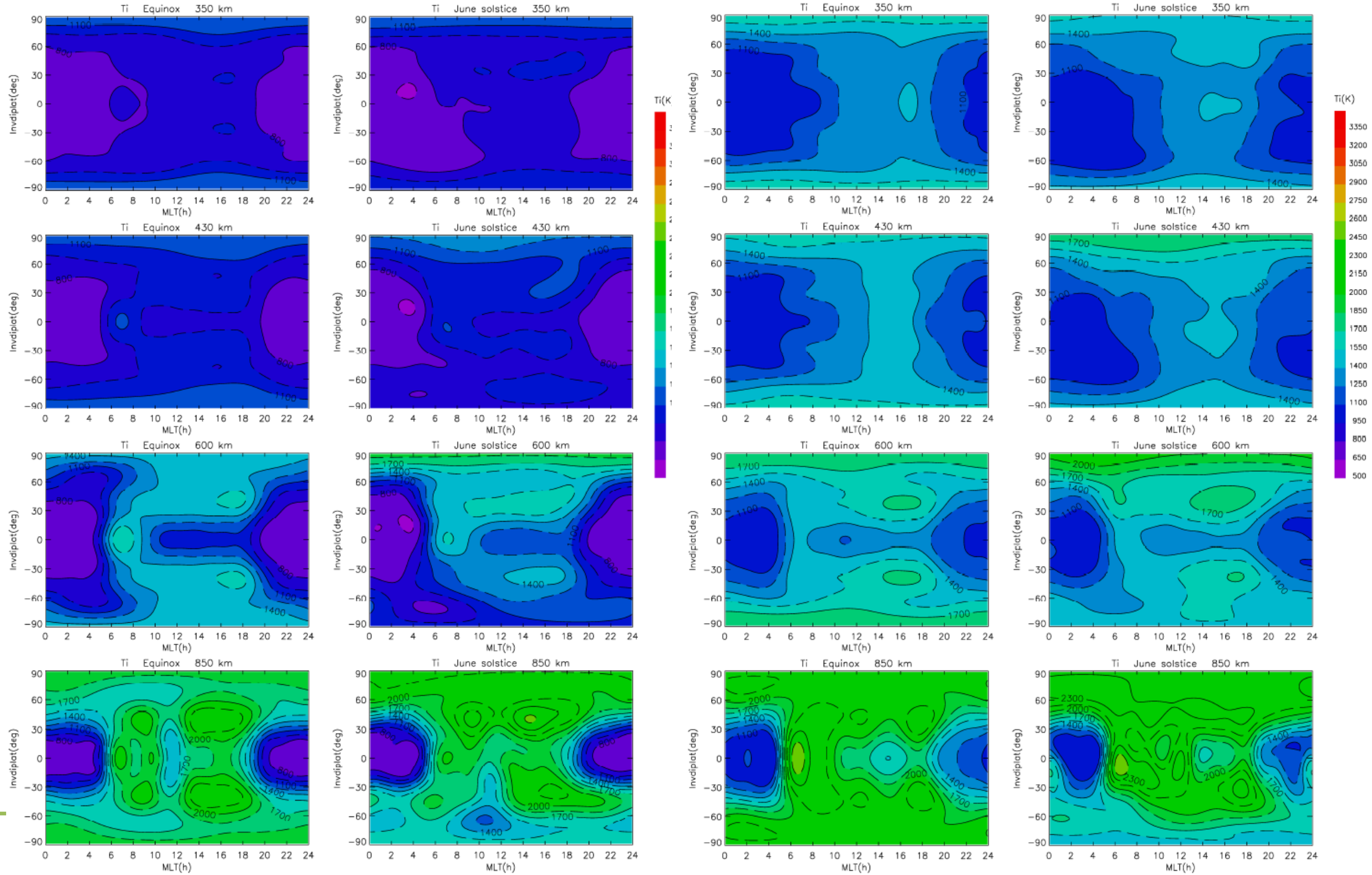

Ti height profiles vs. IRI-2016

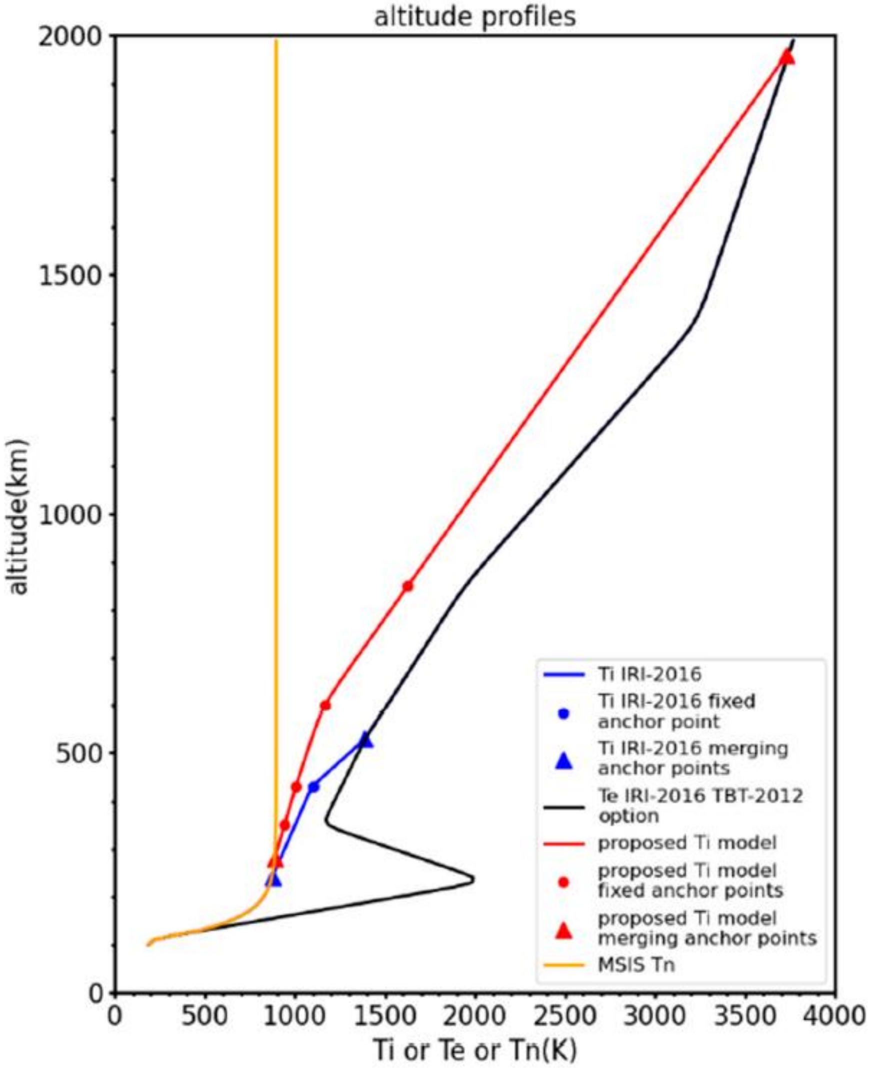

Example of altitude profiles (case for March 21, 2016; PF10.7=92; Solar local time 12 h, geographical latitude=20°; geographical longitude=0°) from the proposed Ti model (red line; 4 red circles represent 4 fixed anchor points with altitudes of 350, 430, 600 and 850 km; 2 red triangles symbolize additional anchor points with variable altitudes - lower one a tangent point on the Tn profile (orange line) and higher one an intersection with the Te profile (black line). The corresponding Ti profile computed from the IRI-2016 model is shown in the blue color (one fixed anchor point at 430 km height - circle; two anchor points for the connection with Tn and Te - triangles).

Summary

- Global models of electron and ion temperatures are included in IRI
- These models include most important dependencies (on latitude, altitude, local time, and solar activity)
- Only limited spatial resolution - up to the 8th order of spherical harmonics
- More data is needed to better describe small scale features (anomalies, enhancements, troughs, longitudinal dependency etc.)